Organic-Inorganic Reaction of Li-Containing thin film: Structure of Lithium Propane Dioxide *via* MLD

Haotian Wang[1], Keith E. Gregorczyk[1], Sang Bok Lee[2], Gary W. Rubloff[1,3], and Chuan-Fu Lin[*, 1, †]

[1]Department of Materials Science and Engineering, University of Maryland, College Park MD 20742

[2]Department of Chemistry and Biochemistry, University of Maryland, College Park, MD 20742

[3]Institute for Systems Research, University of Maryland, College Park, MD 20742

ABSTRACT: In combining organometallic with organic precursors, molecular layer deposition (MLD) offers not only an expanded portfolio of molecular combinations but specifically the possibility of tuning mechanical properties for more robust functionality. This is appealing for applications in energy storage, where ion transport in and out of electrodes causes significant stress/strain cycling. It is particularly opportune for Li ion solid state batteries (LISSBs), where electrode and solid electrolyte structures are usually arranged densely for high power and energy. Despite diverse MLD applications to date, little prior research has been aimed at Li-containing MLD materials and processes. Here we report the MLD growth and process for a lithium-containing organic thin film using lithium tert-butoxide (LiO^{t}Bu) and 1,3-propane diol (PD), leading to an MLD film of lithium propane dioxide, $Li_2O_2C_3H_6$ (LPDO), identified through XPS and ab initio calculations. The growth showed self-limiting behavior for both precursors, with significant nucleation delay before linear growth at 0.23 Å/cycle at 150 ^{o}C, and 0.15 Å/cycle at 200 ^{o}C. XPS-determined stoichiometry was $Li_{1.6}O_{2.2}C_3H_6$ at both 150 ^{o}C and 200 ^{o}C, while additional species, presumably from incomplete reaction, were found at 100 ^{o}C, leading to a notably higher (0.84 Å/cycle) growth rate. The LPDO film showed crystallinity and high surface roughness when grown on crystalline substrate, while on amorphous substrate, amorphous LPDO film with low surface roughness was observed. In addition, high air sensitivity of LPDO film was observed, with Li propyl carbonate and Li carbonate formation under air exposure. Further modification strategies were proposed in order to achieve a MLD or ALD/MLD based solid electrolyte material.

Introduction

Molecular layer deposition (MLD) is a vapor phase material synthesis technique that uses sequential pulses of precursor vapors to deposit organic-inorganic hybrid thin films in a layer by layer manner. As in atomic layer deposition (ALD), the self-limiting growth mechanism enables deposition of ultrathin films over complex geometries with high uniformity and conformality. By employing organic precursors in place of inorganics (e.g., H_2O) to react with typically organometallic precursors, MLD can produce metallic hosts linked by organic moieties whose chemistry can alter a range of material properties, such as electrical conductivity[1,2], thermal conductivity[3,4,5], elastic modulus and hardness[6,7], and crystallinity [8,9]. Thus, in accessing a spectrum of organic functionalities, the MLD approach holds promise for synthesis of tailored functional materials conveying a broadened set of properties.

MLD based metal organic hybrid materials have been used in a variety of applications, including catalysis[10,11,12], microelectronics[13,14,15,16], optics[17], and biomedicines[18,19]. In energy storage application, MLD has been used to deposit battery electrodes[20,21,22] and electrode coatings. The structural flexibility of organic linkers in MLD materials can serve as a vehicle to impart mechanical flexibility to Li-ion batteries (LIBs), with benefits to charge/discharge stability of electrode structures and coatings on them. For example, Piper et al. demonstrated the efficacy of alucone (i.e., aluminum alkoxide) and aluminum dioxybenzene MLD thin films as flexible protection coatings on Si anodes[23,24]. Compared to uncoated Si anode which failed completely by 30^{th} cycle at C/20 rate, alucone coated Si anode showed over 900 mAh/g^{-1} capacity and 99% columbic efficiency at 150^{th} cycle. In addition, by changing the alkoxy functional group to a phenol group, the aluminum dioxybenzene coating showed even further improvement in terms of rate capability and capacity retention of Si anode.

Other than flexible coating, a more interesting topic would be incorporating flexible organic moieties directly into solid electrolyte materials. However, MLD based Li conductor is currently lacking, and as the key component in solid electrolyte for Li ion conduction, Li containing thin film grown by MLD is also

rarely explored. With only two previous reports[25,26], Nisula et al. developed Li terephthalate and Li aryloxide thin films for cathode application. In order to fabricate MLD based electrolyte thin film, polymerized host structure must be obtained[27]. This is challenging for gas phase sythesis but one possibility is to incorporate MLD cycles into existing ALD cycles to build organic moieties onto inorganic electrolytes that have polymer structures. Among a few existing ALD electrolyte materials[28,29,30,31,32,33,34] for Li ion batteries, LiPON and Li polyphosphazene are promising candidates for synthesis of ALD/MLD electrolyte materials, due to their excellent electrochemical properties and polymer structure that allows organic functionalities to be built on.

Following on from two ALD approaches that result in LiPON or related Li polyphosphazenes as solid electrolytes for LISSBs, we report here results from using the same Li source (Li tert-butoxide, LiO^{t}Bu) and an organic linker (1,3-propane diol, PD) in an MLD process. Compared to terephthalate acid and hydroquino used in previous study, PD was chose here due to its lower vapor point and reasonable degree of freedom associated with its three carbon chain. The self-limiting MLD reaction produces a Li propane dioxide (LPDO, also known as Li propane diolate) film, revealing crystallinity, air sensitivity, and high roughness of the LPDO film along the way. Tert-butanol may be a volatile product during MLD reaction. We achieved smooth LPDO films by including a nitrogen plasma component in the initial LPDO layers. This work is a preliminary study for further incorporation into the ALD LiPON and Li polyphosphazene process, to develop a mechanical flexible ALD/MLD solid electrolyte material. This work also represents our first step in achieving MLD electrolyte for 3D-solid state Li ion batteries, as the synthesis of this hybrid LPDO thin film can serve as an organic-inorganic building block for other functionalities to be built upon (e.g. add linkers to tune the materials electrochemical and mechanical properties) and ultimately lead to flexible solid electrolyte materials.

Methods

Experiment

Ultratech Fiji F200 ALD reactor was used for thin film deposition. Single crystal p-type silicon substrates grown in <001> direction were pumped down in a vacuum load lock chamber to a pressure of $1x10^{-3}$ torr. Then, the substrates were transferred to the ALD reactor chamber, where we deposited the LPDO MLD films at 150 °C and 200°C using powder lithium tert-butoxide (LiO^{t}Bu, Sigma-Aldrich, 99.7%) and liquid propanediol (Sigma-Aldrich, 98%). Ultra-high purity Ar gas (Airgas, grade 4.9) was used as carrier gas. During reaction, base pressure of ALD reactor was maintained at 0.1 torr, and a process pressure of 0.2 torr was obtained via Ar gas flow. LiO^{t}Bu was kept in bubbler at 140 °C and delivered to the ALD reaction chamber with 40 sccm argon carrier gas flow and PD was kept at 100 °C to maximize the vapor pressure without thermal decomposition. Process parameters were determined by saturation test, which was conducted on two single crystal silicon wafers. The first test varied PD pulse time from 0s to 10s, with LiO^{t}Bu pulse time fixed at 20s, while the second one varied LiO^{t}Bu pulse time from 0s to 40s, with PD pulse time fixed at 3s. The temperature of carrier gas line was kept at 150 °C for all reaction condition. LPDO MLD films were deposited using precursor saturation doses of 20 sec for LiO^{t}Bu, with 20 sec purge, and 1 sec for PD, with 30 sec purge. For N_2-LPDO seeding layer deposition, 20 sec N_2 remote plasma of 300 W power and with 10 sec purge was added after LiO^{t}Bu and PD pulses. The LPDO film grown on seeding layers used the same process recipe as the original LPDO recipe.

During deposition processes, J.A. Woollam M-2000D spectroscopic ellipsometer with range of wavelength from 360 nm to 990 nm was used to monitor in-situ growth. A Cauchy model with graded layers was used for ellipsometer to capture thickness change of the MLD layer.

After deposition, deposited MLD thin films were transferred through glovebox and UHV load lock to a Kratos Ultra DLD XPS system. Survey spectra were collected without charge neutralization by using monochromatic Al $K\alpha$ X-ray source in hybrid lens mode with a step size of 1eV and pass energy of 160 eV. The incident angle of XPS was 54.7°, with detector angle normal to the substrate. Then, high-resolution core level XPS spectrum were collected in hybrid lens mode with step size of 0.1 eV and pass energy of 20

eV. Core level XPS data were analyzed using CasaXPS with peaks fitted by (70%)Gaussian-(30%)Lorentzian line shape and Shirley background. All high res XPS spectrum were calibrated by assigning C-C bond to 285 eV in C1s spectra.

XRD was performed on Bruker D8 advance discover system with LynxEye PSD detector and Ni β-filter. The X-ray radiation was generated from Cu Kα source(1.54A), the characterization time for each XRD measurement was 30 minutes, scanning from angle 2θ=5° to 55°. AFM was conducted on a NT-MDT NTEGRA Spectra system in tapping mode, at a scanning rate of 1 μm/s. Samples for XRD and AFM measurements were not coated with additional protection layer.

Computational detail

Ab initio simulation of XPS spectra was done using Gaussian 09. Valence XPS simulation method was adopted from Dedryvere et al[42]. Same method and basis set, i.e. restricted Hartree-Fock method and 6-311+G (d,p) basis set, were used for simulation, along with Koopman's theorem to determine the monoelectronic energy of molecular orbitals (MOs). Optimized geometry of LPDO dimer structure was obtained by gradient method and lowest energy configuration was verified through frequency calculation. Gelius intensity equation was applied to predict the photoelectron intensity from each MO:

$$I_j \approx (2 + \frac{\beta_j}{2}) \sum_{i\ AO} P_{j,i}\alpha_i$$

Where i represents the i th atomic orbital, β_j is an asymmetry factor, $P_{j,i}$ are weight contribution of the i th AO to the j th MO, and α_i is the atomic photoionization cross-section of the ith AO. The α_i values used in the study are O_{2s}=0.14, O_{2p}=0.0193, C_{2s}=0.0477, C_{2p}=0.0015, Li_{2s}=0.0008, and H_{1s}=0. The obtained intensity from each MO was then used to construct valence XPS spectra. For comparison with experiment data, each MO peak was generated with a funcational shape made up of a combination of 70% Gaussian and 30% Lorentzian with a fixed FWHM (1.6 eV). The energy scale of the simulated spectra was divided by 1.3 to account for the relaxation and correlation effects that were ignored in Koopman's theorem, and

the HOMO level was shifted to align with the first peak in the experimental valence spectrum, in order to compensate for different reference.

The core level XPS spectra simulation used self-consistent field method(ΔSCF). This method calculate core electron ionization energy based on the difference of energy between initial state, neutrally charged ground state, and final state, i.e. singly charged excited state. Second order Møller-Plesset perturbation theory (MP2) was used to predict electron correlation terms that were ignored in Hartree-Fock. The general accuracy of calculating initial ground state energy using MP2 method is discussed previously, which is crucial for prediction of binding energy shift. In the final state calculation, frozen core hole (FCH) approach was used, to prevent the collapse of wave function at excited state to ground state, while additional scalar relativistic effect was considered for Li core electron excitation calculation.

Results and discussion

In situ spectroscopic ellipsometry was employed extensively to monitor MLD growth for identifying process parameters for MLD synthesis using LiO^{t}Bu and PD. As shown in Figure 1a, both precursors exhibited saturating dose levels at 150^{o}C, i.e. self-limiting adsorption/reaction after 10s for LiO^{t}Bu and 1s for PD, as expected for MLD behavior. The growth per cycle (GPC) under saturation conditions converged to ~0.23 Å/cycle. The slight difference of converged GPC for two precursors is likely due to different surface condition of Si substrate for two saturation tests. In addition, considering the molecular size of Propanediol is ~7A, the saturated GPC is low, indicating self-terminated reaction happened during the growth.

With supply of saturated dosage of both precursors, a growth profile of the MLD process is shown in figure 1(b). A nucleation delay is evident in the first ~100 cycles, after which growth becomes linear. This delayed growth suggests initial island growth associated with a nucleation delay at the initial stage. In addition, the first 6-8 cycles (~2 Å) of growth appear rapid as seen in figure 1(b), although extracting accurate GPC behavior in this range from spectroscopic ellipsometry is challenging. Nevertheless, the raw data for the ellipsometric parameter, delta function, as shown in figure 1(c), reveals a rather sharp change over these

early cycles, consistent with early findings in ALD growth of LiPON[32]. This might result from chemical and/or optical differences reflecting the initial surface reaction that prepares the surface for alternating-precursor MLD growth, as indicated in the step I in figure 3.

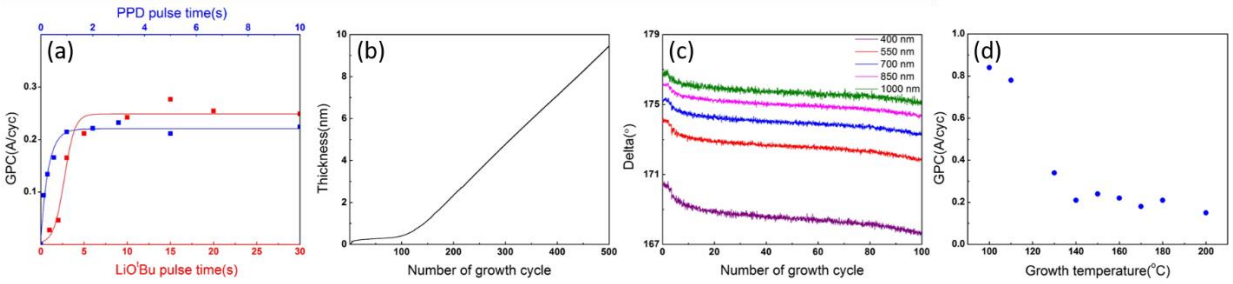

Figure 1. (a) Growth-per-cycle (GPC) with different pulse time of LiO^{t}Bu and PD at 150^{o}C. (b) Growth profile of LPDO at 150^{o}C. (c) Delta profiles during LPDO growth in the first 100 cycles obtained from growth shown in (b) the color codes show the delta profiles with various wavelength of light. (d) GPC at different growth temperature.

The MLD growth rate over the temperature range from 100^{o}C to 200^{o}C was measured, as shown in Figure 1(d). The GPC stabilized to around 0.2 Å/cycle in the range of temperature between 140-180^{o}C, while below 140 ^{o}C, the GPC is substantially larger, reaching 0.84 Å/cycle at 100^{o}C. The high growth rate suggests condensation of LiO^{t}Bu and PD precursors, which will be discussed in the next section.

Chemical structure

X-ray Photoemission Spectroscopy (XPS) - Core Levels

The chemical structure of the deposited MLD film was characterized by X-ray photoelectron spectroscopy (XPS) carried out on samples that were grown for 200 cycles (100^{o}C) and 500 cycles (150^{o}C and 200^{o}C). As shown in Figure 2, the core level XPS spectrum were collected at three different processing temperatures-100, 150, and 200^{o}C. Similar features were seen for all three growth temperatures. The O 1s

peaks at 533.4 eV and 531.2 eV were attributed to Si-O and C-O-Li bonds[34,35] respectively. The C 1s spectrum shows two peaks at 285 eV and 286.4 eV, which were assigned to the center carbon (C-C) and end carbons (C-O) in the carbon backbone of MLD film. Noticeably, the peak-area ratio between these two carbon is C-C : C-O ≈ 1: 2, which is consistent with the atomic ratio of carbon in PD molecular structure, so that the XPS quantification suggests that the PD structure is preserved in the reaction product thin film. The Li 1s spectrum exhibits a primary peak at 55.8 eV, attributed to O-Li bonding[34,56].

Additional minor peaks are required to model the XPS core level lineshapes - for 100°C growth only - in Figure 2, all indicated by "*" and including O 1s at 531.9 eV, C 1s at 287.6 eV, and Li 1s at 57.1 eV binding energies. Since these are indicated only for the low temperature (100 °C) growth condition, we attribute these to configurations unrepresentative of the full MLD reaction, e.g. weakly bonded species from incomplete MLD reaction or unreacted precursor species.

From quantitative core level XPS analysis, as shown in Table 1, the stoichiometry of the product is $Li_{1.6}O_{2.2}C_3H_6$. This is close to the $Li_2O_2C_3H_6$ composition of LPDO, which we therefore identify as the solid MLD reaction product. This implies that tert-butanol (LiO^{t}Bu with H replacing the Li) would likely be the primary gaseous reaction product, and demonstrates that the MLD process is feasible to synthesize highly reactive LDPO via alternated gas-phase chemistry.

A surface reaction mechanism is proposed based on the above analysis, as shown in Figure 3. The first few cycles, leading to the initially faster change in ellipsometric delta function (Figure 1(c)), may correspond to the initial formation of O-Li surface bonds shown as Step I. Subsequently Step II and III involve reaction with the LiO^{t}Bu pulse and the PD pulse respectively, either as nucleation-controlled island growth (up to ~100 cycles) or afterwards as a continuous film. The tert-butanol product is depicted in the figure.

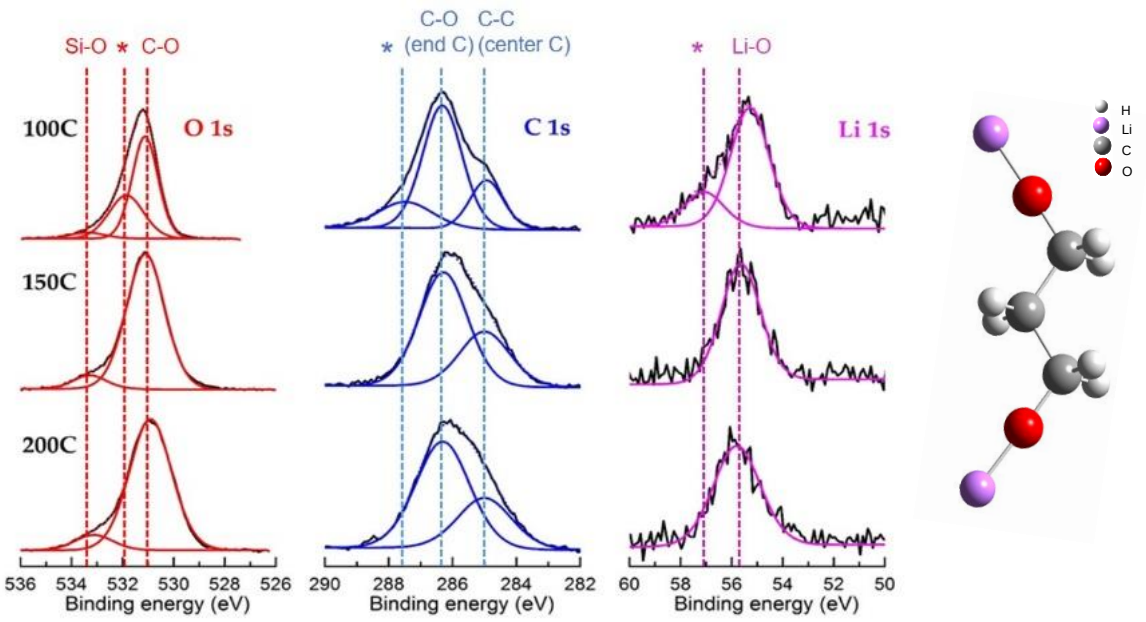

Figure 2. Core level XPS of lithium propane oxide film resulting from LiO^{t}Bu and PD MLD process. ("" designates additional features that may reflect weakly bonded minor parasitic side products, incompletely reacted)*

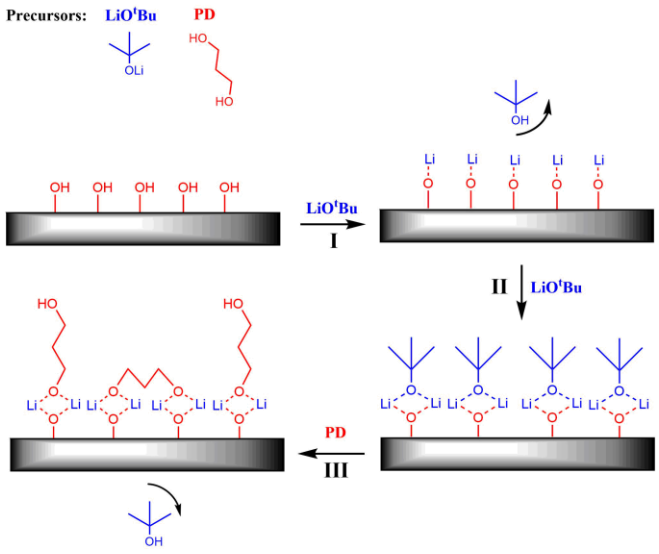

Figure 3. Inferred reaction mechanism for MLD lithium propane oxide from LiO^{t}Bu and PD, showing (I) pre-nucleation and then MLD growth during (II) LiO^{t}Bu dose (III) PD dose and possible double reactions indicated by results of ellipsometry measurement.

Ab-initio calculations

X-ray Photoemission Spectroscopy (XPS) – Core level spectra

The chemical shifts and peak assignments were also examined by ab-initio calculation of core level and valence band structures. First, to reflect the core level electron bonding environment that is likely to occur in building an MLD thin film from LiO^{t}Bu, we chose a monomer structure formed from LiO^{t}Bu with PD-derived linkers, as depicted in Figure 3. Using self-consistent field method with second order Møller-Plesset perturbation theory (MP2) gave the results shown in Table 1. The general accuracy of this calculation method to predict core level electron binding energy is discussed elsewhere[36,37,38,39,40]. A good match between experiment and calculation was observed, with less than 0.1 eV B.E. difference in C 1s and O 1s, as seen in Table 1. Additional considerations were taken for Li 1s simulation, namely a scalar relativistic effect[41] involving orbital contraction/expansion was included. Note that without this assumption, peak position of Li 1s is ~4eV higher than measured in experiment. This issue is highlighted (*) by the computed Li 1s binding energy being shown in Table 1.

	O 1s	C 1s	Li 1s
Peak assignment (Experiment)	531.2 eV	285 & 286.4 eV	55.8 eV
Peak assignment (Calculation_ΔSCF)	531.1 eV	285 & 286.5 eV	55.2 eV *
Atomic ratio (Experiment)	2.2	3	1.6
Atomic ratio (Ideal structure)	2	3	2

Table 1. Comparison of experiment and theory. Atomic ratios and XPS binding energies derived from quantitative XPS analysis and from ab-initio calculation.

Ex-situ X-ray Photoemission Spectroscopy (XPS) - Valence Band Spectra

Valence band XPS spectra were also measured as a complementary fingerprint for identifying the MLD reaction product. These results are shown in Figure 4 with comparison to the ab-initio calculations of valence band density of states, following Koopman's theorem to relate electron binding energies to density of occupied states.

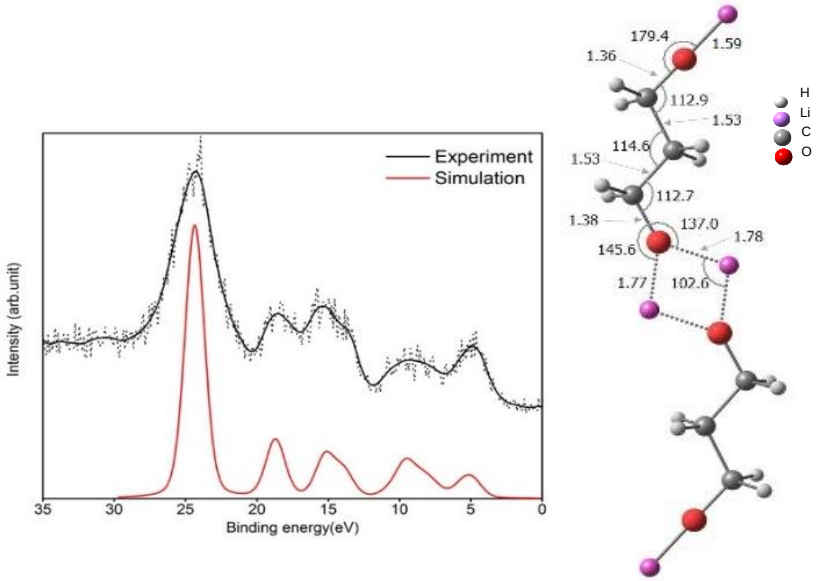

Figure 4. Valence band XPS spectra and simulated valence density of states for the dimer model of lithium propane dioxide (right).

By adjusting binding energy zero between the experimental and calculated valence band spectra, a comparison of relative shapes and positions of the occupied density of states can be made. The result is a striking similarity between the experiment valence band XPS spectra and the computed density of states, suggesting that the dimer model in Figure 4 well describes the valence structure and that $Li_2O_2C_3H_6$ (or the dimer $Li_4O_4C_6H_{12}$) - lithium propane dioxide, LPDO - is the MLD reaction product.

Material Stability

LPDO showed high reactivity when exposed to air, first transforming into Li propyl carbonate (LiPC) and then into Li_2CO_3. We identified these products from their valence (Figure 5) and core level (Figures S1 and S2) XPS spectra. The valence XPS spectra of air exposed LPDO films sequentially matched valence spectra for LiPC and Li_2CO_3 as reported by Dedryvere et al.[42], who attributed the peaks at 15.4 eV and 18.8 eV, as well as the shoulder at 13.5 eV, as indicators of the propyl functional group in Li alkylcarbonate. With increasing amount of air exposure, the $–CH_2$ of propyl group in the film disappears, suggesting that propane-dioxide functional group becomes propane-diol and enters the gas phase, leaving Li_2CO_3 in the film.

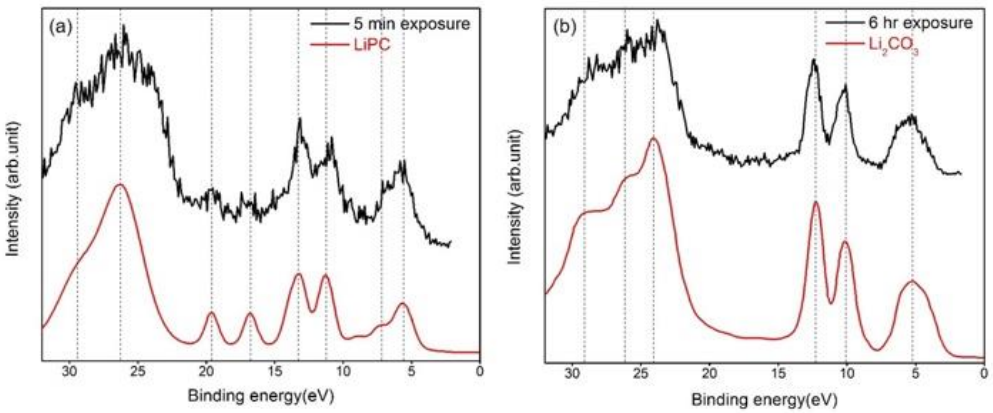

Figure 5. Valence XPS spectrum of LPDO exposed to air by 5 minutes to form (a) Li propyl carbonate (LiPC), and 6 hours to form (b) Li_2CO_3. Reference spectra obtained from Dedryvere[42].

Crystallinity and film roughness

Crystallinity of LPDO MLD film was studied by X-ray diffraction (XRD), as shown in figure 6 (a). For LPDO film, five diffraction peaks were observed, while three peaks at 2θ=32.9°, 47.7°, and 54.6° were attributed to Si substrate, annotated as "*". The other two diffraction peaks at 2θ=10.4° and 20.1° were assigned to (100) and (200) plane in the MLD film, respectively. The assignment of these diffraction peaks

were based on the molecular size of LPDO from ab-initio calculation. The spacing between Li ions in LPDO is 6.4A, which is lower than the planar spacing corresponding to the diffraction peak at 2θ=10.4° (8.46A), even it is the lowest index plane. However, considering that LPDO is air sensitive and transforms into LiPC in air, the first peak is possibly attributed to LiPC, which has molecular size of ~8.6A based on ref 43. Therefore, the peak at 2θ=10.4° was assigned as (100) in LiPC, and peak at 2θ=20.1° was assigned as (200) due to half of planar spacing. To confirm that the crystallinity of the MLD film was not introduced by reaction with air, remote nitrogen plasma treatment was added to the LPDO MLD process in order to amorphize the . At each cycle of N_2-LPDO process, N_2 plasma was pulsed after PD pulse. The energetic N_2 plasma tends to interact with PD precursor and forms covalent bonding with carbon in PD, as shown in figure S3. After 10 cycles of N_2-LPDO growth, LPDO film was then grown on this amorphous seeding substrate. Chemical identity of the LPDO film grown on seeding layer was identical to pure LPDO, as shown in figures S4-S6, along with growth behavior of LPDO grown on N_2-LPDO seeding layer, while the LPDO film turned into amorphous. Therefore, the crystallinity of the MLD film is highly dependent on the crystallinity of substrate. The N_2 plasma was chosen as opposed to other plasma, such as O_2 and Ar plasma, since it is less aggressive, it doesn't oxidize the organic linker. Besides lower crystallinity, surface roughness of LPDO grown on seeding layer was also reduced compared to bare LPDO film, as shown in figure 6 (b) and (c). The RMS surface roughness dropped from 20.3nm to 2.1nm when it was grown on seeding layer, which strength the previous point that the LPDO film growth is highly dependent on the substrate condition.

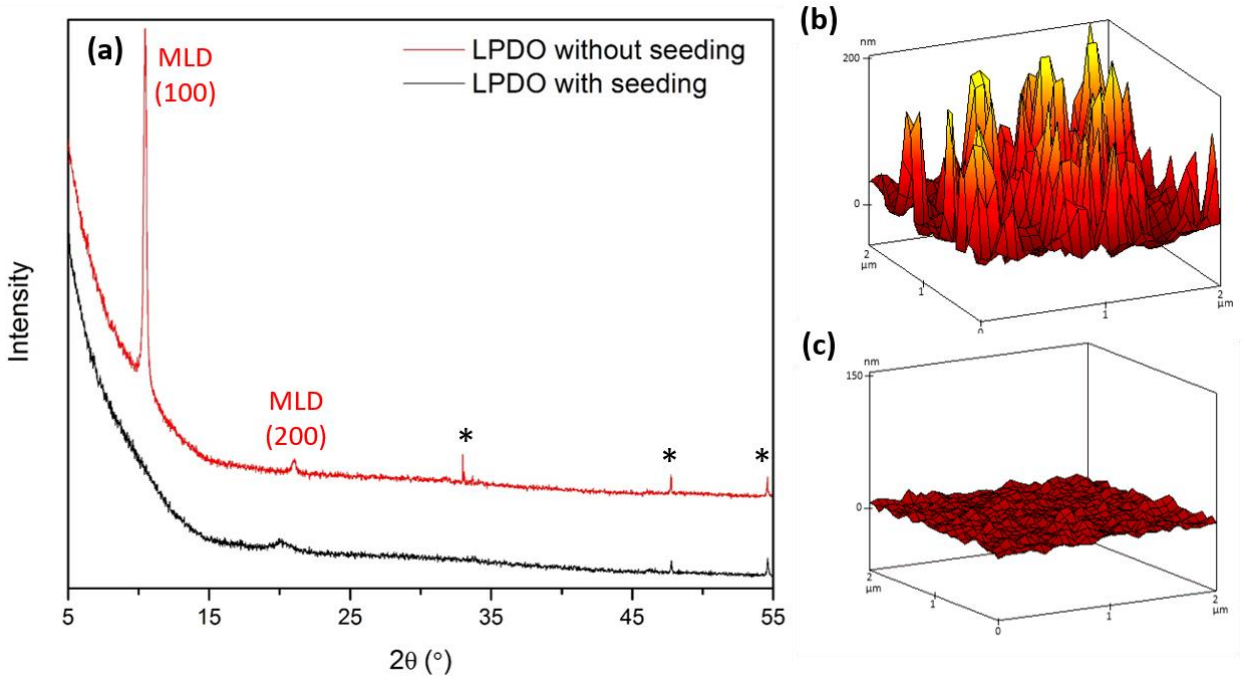

*Figure 6. (a) XRD of LPDO MLD film grown at 150°C with and without N_2-LPDO seeding layer. The * indicates diffraction peaks originated from Si <100> substrate. (b) AFM of LPDO MLD film, and (c) LPDO MLD film grown on N_2-LPDO seeding layer.*

Conclusion

This work demonstrates the synthesis of a Li-containing organic thin film using organic-inorganic MLD reaction between LiO^{t}Bu and PD. The MLD growth showed self-limiting behavior and island growth mode, along with a temperature window from 140 to 200°C. The low growth rate (0.23A/cycle) of the MLD process within temperature window suggests self-terminating reaction during the process. From XPS quantification and ab-initio calculation, we identify the chemical structure of the product as Li propane dioxide structure, with stoichiometry $Li_{1.6}O_{2.2}C_3H_6$ as close approximation to $Li_2O_2C_3H_6$. We therefore concluded that the proton exchange reaction between LiO^{t}Bu and PD was robust, with no side products observed in temperature range 140-200 °C. The LPDO film showed crystallinity and highly oriented growth on crystalline silicon wafer, indicating a nature of strong ionic bonding between Li ions and propane-oxide anions.

This work is a significant step toward hybrid inorganic-organic solid electrolyte for LISSBs. However, due to the crystallinity of LPDO film, it will only be investigated as a sub-cycle combined with LiPON ALD process, to form ALD/MLD hybrid electrolytes. In order to fabricate MLD based electrolyte materials, adding additional organic linkers to enable crosslinking in the structure is necessary. We therefore also aim to use LPDO as an initial building block to incorporate the third precursors, during or after the synthesis, to tune its mechanical and electrochemical properties. The potential advantage of tailorable mechanical and electrochemical properties of LPDO derived materials can enable stabilized electrode-electrolyte interface, high performance, and long cycle life LISSBs.

AUTHOR INFORMATION

Corresponding Author

* Chuan-Fu Lin: linc@cua.edu

Present Addresses

† Department of Mechanical Engineering, the Catholic University of America

Author Contributions

HW, CFL, and GWR conceived the idea and designed experiments, HW, CFL, KEG, SBL and GWR analyzed and interpreted experiment data. HW, CFL, and GWR co-wrote the manuscript. All authors contributed in discussion of the work and manuscript.

Additional information

Supporting Information is available for this paper.

Competing financial interests

The authors declare no competing financial interests.

Supporting information

Core level XPS of LPDO exposed to air, growth profile of LPDO grown on N_2-LPDO seeding layer, core level XPS of LPDO grown on N_2-LPDO seeding layer.

ACKNOWLEDGMENT

The primary motivation and effort in this work has been supported by the U.S Department of Energy, Office of Science, Office of Basic Energy Sciences under Award Number DESC0017620. Completion of the work and manuscript has been partially supported by Nanostructures for Electrical Energy Storage (NEES), an Energy Frontier Research Center funded by U.S Department of Energy, Office of Science, Office of Basic Energy Sciences under Award Number DESC0001160. We acknowledge the support of University of Maryland Nanocenter and its AIMLab.

REFERENCES

1. Lushington, A.; Liu, J.; Bannis, M.; Xiao, B.; Lawes, S.; Li, R.; Sun, X. A novel approach in controlling the conductivity of thin films using molecular layer deposition. *Applied Surface Science: Part B*, **2015**, *357*, 1319-1324.

2. Yoon, B.; Lee, B.; George, S. Highly conductive and transparent hybrid organic-inorganic zincone thin films using atomic and molecular layer deposition. *Journal of Physical Chemistry C*, **2012**, *116*, 24784-24791.

3. Niemelä, J.; Karttunen, A.; Karppinen, M. Inorganic–organic superlattice thin films for thermoelectrics. *Journal of Materials Chemistry C*, **2015**, *3*, 10349-10361.

4. Tynell, T.; Karppinen, M. Atomic layer deposition of ZnO: A review. *Semiconductor Science and Technology*, **2014**, *29*, 043001-043001.

5. Liu, J.; Yoon, B.; Kuhlmann, E.; Tian, M.; Zhu, J.; George, S.; Lee YC.; Yang, R. Ultralow thermal conductivity of atomic/molecular layer-deposited hybrid organic-inorganic zincone thin films. *Nano Letters*, **2013**, *13*, 5594-5599.

6. Lee, B.; Yoon, B.; Anderson, V.; George, S. Alucone alloys with tunable properties using alucone molecular layer deposition and Al_2O_3 atomic layer deposition. *Journal of Physical Chemistry C*, **2012**, *116*, 3250-3257.

7. Miller, D.; Foster, R.; Zhang, Y.; Lu, Z.; Yang, R.; Lee, Y.; Dunn, M.; Jen, S.; Bertrand, J.; Seghete, D.; et al. The mechanical robustness of atomic layer and molecular layer deposited coatings on polymer substrates. *Journal of Applied Physics*, **2009**, *105*.

8. Bergsman, D.; Closser, R.; Tassone, C.; Clemens, B.; Nordlund, D.; Bent, S. Effect of backbone chemistry on the structure of polyurea films deposited by molecular layer deposition. *Chemistry of Materials*, **2017**, *29*, 1192-1203.

9. Tanskanen, A.; Karppinen, M. Iron-terephthalate coordination network thin films through in-situ atomic/molecular layer deposition. *Scientific Reports*, **2018**, *8*.

10. MacIsaac, C.; Schneider, J.; Closser, R.; Hellstern, T.; Bergsman, D.; Park, J.; Liu, Y.; Sinclair, R.; Bent, S. Atomic and molecular layer deposition of hybrid mo-thiolate thin films with enhanced catalytic activity. *Advanced Functional Materials*, **2018**, *28*.

11. Gould, T.; Izar, A.; Weimer, A.; Falconer, J.; Medlin, J. Stabilizing ni catalysts by molecular layer deposition for harsh, dry reforming conditions. *ACS Catalysis*, **2014**, *4*, 2714-2717.

12. Sarkar, D.; Ishchuk, S.; Taffa, D.; Kaynan, N.; Berke, B.; Bendikov, T.; Yerushalmi, R. Oxygen-deficient titania with adjustable band positions and defects; molecular layer deposition of hybrid organic–inorganic thin films as precursors for enhanced photocatalysis. *The Journal of Physical Chemistry C*, **2016**, *120*, 3853-3862.

13. Zhou, W.; Leem, J.; Park, I.; Li, Y.; Jin, Z.; Min, Y. Charge trapping behavior in organic–inorganic alloy films grown by molecular layer deposition from trimethylaluminum, p-phenylenediamine and water. *Journal of Materials Chemistry*, **2012**, *22*, 23935-23935.

14. Cha, S.; Park, A.; Lee, K.; Im, S.; Lee, B.; Sung, M. Pentacene thin-film on organic/inorganic nanohybrid dielectrics for zno charge injection memory transistor. *Organic Electronics*, **2010**, *11*, 159-163.

15. Lee, B.; Lee, K.; Im, S.; Sung, M. Monolayer-precision fabrication of mixed-organic-inorganic nanohybrid superlattices for flexible electronic devices. *Organic Electronics*, **2008**, *9*, 1146-1153.

16. Lee, B.; Im, K.; Lee, K.; Im, S.; Sung, M. Molecular layer deposition of ZrO_2-based organic-inorganic nanohybrid thin films for organic thin film transistors. *Thin Solid Films*, **2009**, *517*, 4056-4060.

17. Lee, B.; Anderson, V.; George, S. Molecular layer deposition of zircone and ZrO_2/zircone alloy films: Growth and properties. *Chemical Vapor Deposition*, **2013**, *19*, 204-212.

18. Yoshimura, T.; Yoshino, C.; Sasaki, K.; Sato, T.; Seki, M. Cancer therapy utilizing molecular layer deposition and self-organized lightwave network: Proposal and theoretical prediction. *Ieee Journal on Selected Topics in Quantum Electronics*, **2012**, *18*, 1192-1199.

19. Momtazi, L.; Dartt, D.; Nilsen, O.; Eidet, J. Molecular layer deposition builds biocompatible substrates for epithelial cells. *Journal of Biomedical Materials Research Part A*, **2018**, *106*, 3090-3098.

20. Nisula, M,; Karppinen, M. Atomic/molecular Layer Deposition of Lithium Terephthalate Thin Films As High Rate Capability Li-Ion Battery Anodes. *Nano Letters*, **2016**, *16*, 1276–1281.

21. Bergsman, D.; Baker, J.; Closser, R.; Maclsaac, C.; Lillethorup, M.; Strickler, A.; Closser, R.; Godet, L.; Bent, S.F. Structurally stable manganese alkoxide films grown by hybrid molecular layer deposition for electrochemical applications. *Advanced Functional Materials*, **2019**, *29*, 1904129–1904129.

22. Van, D.; Mattelaer, F.; Dendooven, J.; Detavernier, C. Molecular layer deposition of "vanadicone", a vanadium-based hybrid material, as an electrode for lithium-ion batteries. *Dalton Transactions (cambridge, England : 2003)*, **2017**, *46*, 4542-4553.

23. Piper, D. M.; Travis, J. J.; Young, M.; Son, S.-B.; Kim, S. C.; Oh, K. H.; George, S. M.; Ban, C.; Lee, S.H. Reversible High-Capacity Si Nanocomposite Anodes for Lithium-Ion Batteries Enabled by Molecular Layer Deposition. *Advanced Materials*, **2014**, *26*, 1596–1601.

24. Piper, D.M.; Lee, Y.; Son, S.; Evans, T.; Lin, F.; Nordlund, D.; Xiao, X.; George, S.; Lee, S.; Ban, C. Cross-linked aluminum dioxybenzene coating for stabilization of silicon electrodes. *Nano Energy*, **2016**, *22*, 202-210.

25. Nisula, M.; Karppinen, M. Atomic/molecular layer deposition of lithium terephthalate thin films as high rate capability li-ion battery anodes. *Nano Letters*, **2016**, *16*, 1276-81.

26. Nisula, M.; Linnera, J.; Karttunen, A.; Karppinen, M. Lithium aryloxide thin films with guest-induced structural transformation by ALD/MLD. *Chemistry - a European Journal*, **2017**, *23*, 2988-2992.

27. Zhang, H.; Li, C.; Piszcz, M.; Coya, E.; Rojo, T.; Rodriguez-Martinez, L.; Zhou, Z. Single lithium-ion conducting solid polymer electrolytes: Advances and perspectives. *Chemical Society Reviews*, **2017**, *46*, 797-815.

28. Liu, J.; Banis, M.; Li, X.; Lushington, A.; Li, R.; Sun, X.; Cai, M.; Sham, T. Atomic layer deposition of lithium tantalate solid-state electrolytes. *Journal of Physical Chemistry C*, **2013**, *117*, 20260-20267.

29. Cao, Y.; Meng, X.; Elam, J. Atomic layer deposition of Li_xAl_yS solid-state electrolytes for stabilizing lithium-metal anodes. *Chemelectrochem*, **2016**, *3*, 858-863.

30. Xie, J.; Sendek, A.D.; Cubuk, E.D.; Zhang, X.; Lu, Z.; Gong, Y.; Wu, T.; Shi, F.; Liu, W.; Reed, E.J.; et al. Atomic Layer Deposition of Stable Lialf4 Lithium Ion Conductive Interfacial Layer for Stable Cathode Cycling. *Acs Nano*, **2017**, *11*, 7019–7027.

31. Kazyak, E.; Davis, A.L.; Yu, S.; Sanchez, A.J.; Lasso, J.; Bielinski, A.R.; Thompson, T.; Sakamoto, J.; Siegel, D.J.; Dasgupta, N.P.; et al. Atomic Layer Deposition and First Principles Modeling of Glassy Li3bo3-Li2co3 Electrolytes for Solid-State Li Metal Batteries. *Journal of Materials Chemistry A*, **2018**, *6*, 19425–19437.

32. Kozen, A. C.; Pearse, A. J.; Lin, C.F.; Noked, M.; Rubloff, G. W. Atomic Layer Deposition of the Solid Electrolyte Lipon. *Chemistry of Materials*, **2015**, *27*, 5324–5331.

33. Pearse, A.J.; Schmitt, T.E.; Lin, C.F.; Rubloff, G.; Gregorczyk, K.E.; Gerasopoulos, K.; Kozen A.C.; Fuller, E.J.; El-Gabaly, F.; Talin, A.A. Nanoscale Solid State Batteries Enabled by Thermal Atomic Layer Deposition of a Lithium Polyphosphazene Solid State Electrolyte. *Chemistry of Materials*, **2017**, *29*, 3740–3753.

34. Lu, Y.; Crumlin, E.; Veith, G.; Harding, J.; Mutoro, E.; Dudney, N.; Liu, Z.; Shao-Horn, Y.; In situ ambient pressure x-ray photoelectron spectroscopy studies of lithium-oxygen redox reactions. *Scientific Reports*, **2012**, *2*.

35. Marchini, F.; Herrera, S.; Torres, W.; Tesio, A.; Williams, F.; Calvo, E.; Surface study of lithium-air battery oxygen cathodes in different solvent-electrolyte pairs. *Langmuir : The ACS Journal of Surfaces and Colloids*, **2015**, *31*, 9236-9245.

36.Giesbers, M.; Marcelis, A.; Zuilhof, H. Simulation of XPS C1s spectra of organic monolayers by quantum chemical methods. *Langmuir*, **2013**, *29*, 4782-4788.

37. Besley, N.; Gilbert, A.; Gill, P. Self-consistent-field calculations of core excited states. *The Journal of Chemical Physics*, **2009**, *130*, 124308.

38. Bagus, P.; Illas, F.; Pacchioni, G.; Parmigiani, F. Mechanisms responsible for chemical shifts of core-level binding energies and their relationship to chemical bonding. *Journal of Electron Spectroscopy and Related Phenomena*, **1999**, *100*, 215-236.

39. Bagus, P.; Ilton, E.; Nelin, C. The interpretation of xps spectra: Insights into materials properties. *Surface Science Reports*, **2013**, *68*, 273-304.

40. Kotsis, K.; Staemmler, V. Ab initio calculations of the O1s XPS spectra of ZnO and Zn oxo compounds. *Physical Chemistry Chemical Physics (incorporating Faraday Transactions)*, **2006**, *8*, 1490-1498.

41. Hill, J.; Peterson, K. Gaussian basis sets for use in correlated molecular calculations. xi. pseudopotential-based and all-electron relativistic basis sets for alkali metal (K-Fr) and alkaline earth (Ca-Ra) elements. *The Journal of Chemical Physics*, **2017**, *147*, 244106-244106.

42. Dedryvère, R.; Gireaud, L.; Grugeon, S.; Laruelle, S.; Tarascon, J.; Gonbeau, D. Characterization of lithium alkyl carbonates by x-ray photoelectron spectroscopy: Experimental and theoretical study. *The Journal of Physical Chemistry. B*, **2005**, *109*, 15868-15875.